Available online at www.sciencedirect.com
SCIENCE DIRECT®
ELSEVIER
European Journal of Mechanics B/Fluids 22 (2003) 179–198

The effect of fine structure on the stability of planar vortices

Ian M. Hall [1], Andrew P. Bassom *, Andrew D. Gilbert

School of Mathematical Sciences, University of Exeter, Exeter, EX4 4QE, UK

Received 22 May 2002; accepted 3 February 2003

Abstract

This study considers the linear, inviscid response to an external strain field of classes of planar vortices. The case of a Gaussian vortex has been considered elsewhere, and an enstrophy rebound phenomenon was noted: after the vortex is disturbed enstrophy feeds from the non-axisymmetric to mean flow. At the same time an irreversible spiral wind-up of vorticity fluctuations takes place. A top-hat or Rankine vortex, on the other hand, can support a non-decaying normal mode.

In vortex dynamics processes such as stripping and collisions generate vortices with sharp edges and often with bands or rings of fine scale vorticity at their periphery, rather than smooth profiles. This paper considers the stability and response of a family of vortices that vary from a broad profile to a top-hat vortex. As the edge of the vortex becomes sharper, a quasi-mode emerges and vorticity winds up in a critical layer, at the radius where the angular velocity of the fluid matches that of a normal mode on a top-hat vortex. The decay rate of these quasi-modes is proportional to the vorticity gradient at the critical layer, in agreement with theory. As the vortex edge becomes sharper it is found that the rebound of enstrophy becomes stronger but slower.

The stability and linear behaviour of coherent vortices is then studied for distributions which exhibit additional fine structure within the critical layer. In particular we consider vorticity profiles with 'bumps', 'troughs' or 'steps' as this fine structure. The modified evolution equation that governs the critical layer is studied using numerical simulations and asymptotic analysis. It is shown that depending on the form of the short-scale vorticity distribution, this can stabilise or destabilise quasi-modes, and it may also lead to oscillatory behaviour.

Keywords: Vortex dynamics; Stability; Critical layer; Quasi-mode

1. Introduction

In two-dimensional turbulence the vorticity distribution is dominated by isolated coherent vortices [1–3]. These move in the plane, and between collisions behave approximately like a collection of point vortices with the same circulations [4]. In terms of the internal dynamics of a given vortex, once its motion is factored out, it is subject to a time-dependent straining field from the other vortices, at a leading approximation. This raises the question of how the vortex responds to an irrotational external forcing, and the related problem of vortex stability. There have been many studies of the stability and behaviour of smooth vortices, but less is known when the vorticity has more complex structure, as can occur through collisions and processes of vortex stripping [5,6]. Vortices which are approximately axisymmetric but have fine structure also occur in other fluid flows, for example three-dimensional turbulence (e.g., [7]), and atmospheric and oceanographic flows (e.g., [8–11]). Motivated by these applications, the aim of this paper is to extend results known for smooth vortices to such complex vortices that are more typical of those seen in many fluid flows.

* Corresponding author.
E-mail address: drew@maths.ex.ac.uk (A.P. Bassom).
[1] Present address: Centre for Applied Microbiology & Research, Porton Down, Salisbury, Wiltshire, SP4 0JG, UK.

0997-7546/03/$ – see front matter
doi:10.1016/S0997-7546(03)00016-5

In [12] the behaviour of a Gaussian vortex in an external strain field was studied both numerically and asymptotically. The focus there is on linear evolution and so an impulsive strain field is used, giving a Green's function for the general response. It is found that during the process of spiral wind-up of fluctuating vorticity [13] there is a noticeable suppression of non-axisymmetric vorticity. This was further explored in [14,15] where a 'rebound phenomenon' is described: when the vortex is strained enstrophy is transferred from the mean, axisymmetric component of the vortex, to the non-axisymmetric components which are subject to spiral wind-up. However during this winding-up process much of the enstrophy is transferred back again; that is, it rebounds. Subsequent papers [16–18] reveal that this is closely connected with the existence of 'quasi-modes' [19] in the vortex, which we will discuss shortly. These processes of spiral wind-up and axisymmetrisation observed for linear perturbations to a Gaussian vortex stand in contrast to the inviscid behaviour of a top-hat vortex [20] (also known as a Rankine or Kida vortex): in a time-dependent strain field this remains elliptical for all times.

The Gaussian (or Lamb) vortex, while it is a solution of the Navier–Stokes equations with smooth vorticity characterised by a single length-scale, is however not that typical of the vortices seen in practical examples [1–3]. For example, the process of vortex stripping [5,6,21] can lead to vortices with sharp edges and weak vorticity around the periphery. This occurs when a vortex is strongly strained (by other vortices in the flow) and vorticity is pulled off from the edge of the vortex in thin sheets; essentially the vorticity is stripped along separatrices of hyperbolic stagnation points in the flow field. If the vortex now relaxes to an approximately axisymmetric distribution, what is left is a vorticity profile with a sharp edge and weak vorticity beyond this edge. This vortex is characterised by two length scales, that of the original vortex, and the width of the edge. If the weak vorticity is smooth (an assumption we later relax below), such a vortex lies somewhere between a Gaussian and the top-hat vortex.

In this paper we begin by setting up a family of vortices with a parameter σ: when $\sigma = 0$ the vortex has a broad profile, but in the limit $\sigma \to 1$ the vortex approaches the top-hat vortex. (The stability of a similar family is studied in [17].) We investigate numerically the evolution of vortices in this family when subjected to impulsive strain, under a linear approximation and in the absence of viscosity. Our aim in Section 2 is to quantify how the rebound effect changes as the vortex edge becomes sharper. We will find that the rebound phenomenon is strengthened in this limit: an increasing amount of vorticity is transferred to the mean from the fluctuating components as σ tends to 1. In this limit the time-scale of the transfer process also grows. Note that we consider impulsive strain, which is idealised; for example in two-dimensional turbulence a vortex is inevitably immersed in a weak strain field generated by the other vortices (varying on a time-scale of the order of the inverse strain), although obviously this becomes stronger when another vortex comes close. Although a paradigm, this is the simplest excitation to use to consider the stability of vortices and the transfers of enstrophy when azimuthal structure is generated. Other strain fields could be used, though our experience is that the rebound of vorticity becomes enhanced in the (adiabatic) limit of slowly varying strain [14,15].

In fact the time-scale of the enstrophy rebound is governed by a 'quasi-mode': this is best understood using the model of Balmforth et al. [16] (hereafter referred to as BLSY) who consider a vortex consisting of a compact core with a weak skirt of vorticity superposed. The core, which could be a top-hat vortex for instance, has vorticity that is strictly zero beyond some radius $r = r_0$ and it can support a normal mode of the form $g(r)\,\mathrm{e}^{\mathrm{i}n\theta - \mathrm{i}n\varpi t}$. The frequency ϖ determines a critical radius r_n where this frequency matches the angular frequency of the fluid motion. If r_n lies outside the compact vortex the mode is undamped; however, if a weak skirt of vorticity is superposed then the mode is damped, or can be destabilised, depending on the vorticity gradient $\omega'(r_n)$ at the critical radius [16–19,22]. In Section 3 we set out relevant theory, based on [16], and confirm that the rebound phenomenon corresponds to the damping of such quasi-modes by measuring the damping rates and comparing with theoretical predictions.

The above theory of quasi-modes relates the damping of a normal mode to the gradient of weak vorticity in a thin critical layer, whose width is asymptotically of the order of $\varepsilon = \omega'(r_n)$. It is based on the assumption that the vorticity distribution is smooth in the critical layer; however owing to vortex interactions a typical structure can have a quite complex vorticity distribution at its periphery. Not only is the stripping mechanism mentioned above important, but two other processes are also of significance. The first is axisymmetrisation: if a strongly perturbed vortex relaxes to axisymmetry (though it does not *always* do this) the final state is often characterised by a coherent vortex, surrounded by a ring of vorticity [23,24]. This effect may also be seen in weakly nonlinear theory: spiral wind-up of vorticity fluctuations is accompanied by a feedback on the mean that can leave behind kinks in the axisymmetric vorticity distribution [14–16]. The second process is that of vortex collision. When two or more vortices interact, a variety of strongly nonlinear processes can take place, one of which is the destruction of a weak vortex and the wrapping of weaker vorticity (of either sign) about a strong vortex [25–28]. This again can lead to a vortex possessing fine scale structure at its periphery including rings of weak vorticity of either sign, with implications for the robustness of the vortex to external disturbances [26].

These various processes lead to vortices with finer scale vorticity, varying within the critical layer, and in this case there will not be a single well-defined value for the vorticity gradient there. (Note that this idea of a critical layer with fine scale vorticity structure within it, has elements in common with studies of 'vorticity defects' [29,30] in which a region of localised vorticity is embedded within a shear flow.) We consider the effect of different types of structure in the critical layer on the stability and behaviour of quasi-modes, within the linear, inviscid approximation. In Section 4 we extend the theory of BLSY to this case, which gives rise to a coupled system of an integral equation and a differential equation; these are studied numerically and asymptot-

ically. We consider a number of possible profiles for the vorticity distribution in the critical layer including localised 'steps', 'bumps' and 'troughs', which we will define below. Depending on the form of the fine-scale vorticity, the quasi-mode can be stabilised or destabilised, and it may also demonstrate oscillatory behaviour. Finally Section 6 offers some concluding discussion.

2. Rebound of enstrophy in a family of vortices

We begin by summarising the governing equations for linear and weakly nonlinear disturbances to a planar vortex; for further background see [12] or [14]. The vorticity equation may be written in the dimensionless form

$$\partial_t \Omega_{\text{total}} + J(\Psi_{\text{total}} + \Psi_{\text{ext}}, \Omega_{\text{total}}) = R^{-1}\nabla^2 \Omega_{\text{total}}, \tag{2.1}$$

$$\nabla^2 \Psi_{\text{total}} = \Omega_{\text{total}}, \qquad \nabla^2 \Psi_{\text{ext}} = 0, \tag{2.2}$$

where R is the Reynolds number, Ω_{total} is the total vorticity, Ψ_{total} the associated stream function and Ψ_{ext} the stream function of the externally imposed irrotational flow. The Jacobian $J(a,b) \equiv r^{-1}(\partial_r a\, \partial_\theta b - \partial_\theta a\, \partial_r b)$ in polar coordinates (r,θ). The split into the two stream functions Ψ_{total} and Ψ_{ext} is fixed by their far field behaviours: Ψ_{total} is generated by the localised vorticity distribution Ω_{total} and grows at most logarithmically as $r \to \infty$. The external stream function Ψ_{ext} can be thought of as generated by distant vortices or moving boundaries, and grows algebraically with r; it can be specified as a harmonic function with arbitrary time-dependence.

Near the vortex Ψ_{ext} can be expanded as the sum of terms of the form $r^n \,\mathrm{e}^{\pm \mathrm{i}n\theta}$, for $n \geqslant 0$. If Ψ_{ext} is generated at some distance from the vortex, the dominant effect on the internal dynamics of a vortex comes from the $n = 2$ term and so we shall henceforth restrict ourselves to the case

$$\Psi_{\text{ext}} = \delta q(t) r^n \,\mathrm{e}^{\mathrm{i}n\theta} + \text{c.c.} \quad (n = 2), \tag{2.3}$$

where 'c.c.' denotes the complex conjugate of the preceding expression. (Although we have fixed $n = 2$, we leave n in below to indicate the general structure of the problem.) The constant δ in the following analysis is considered to be a small parameter, $0 < \delta \ll 1$, since we are considering weak external flow; for an extension of our weakly nonlinear analysis for the Gaussian vortex see [15]. Within (2.3) the function $q(t)$ is complex-valued and determines the time dependence, amplitude and orientation of the external straining flow.

We now expand vorticity in powers of $\delta \ll 1$ as

$$\Omega_{\text{total}} = \Omega_0(r,t) + \delta\big[\omega(r,t)\exp(\mathrm{i}n\theta) + \text{c.c.}\big] + \delta^2\big[\omega_2(r,t)\exp(2\mathrm{i}n\theta) + \text{c.c.} + \Omega_2(r,t)\big] + \mathrm{O}\big(\delta^3\big), \tag{2.4}$$

with a similar form for Ψ_{total}. Note that Ω_i and Ψ_i denote mean, axisymmetric components, while the terms ω_i, ψ_i give the fluctuating, non-axisymmetric components. To keep later notation simple we have omitted a subscript '1' from the order-δ fields ω and ψ.

When this expansion is substituted into (2.1), (2.2) we obtain equations for the mean fields Ω_0, Ω_2 and the azimuthal field ω:

$$\partial_t \Omega_0 = R^{-1}\Delta_0 \Omega_0, \qquad \Omega_0 = \Delta_0 \Psi_0, \tag{2.5}$$

$$\partial_t \omega + \mathrm{i}n\alpha\omega - \mathrm{i}n\beta\big(\psi + qr^n\big) = R^{-1}\Delta_1 \omega, \qquad \omega = \Delta_1 \psi, \tag{2.6}$$

$$\partial_t \Omega_2 - \mathrm{i}nr^{-1}\partial_r\big[\big(\psi + qr^n\big)\omega^*\big] + \text{c.c.} = R^{-1}\Delta_0 \Omega_2, \qquad \Omega_2 = \Delta_0 \Psi_2, \tag{2.7}$$

where

$$\Delta_m \equiv \partial_r^2 + r^{-1}\partial_r - n^2 m^2 r^{-2}, \quad \alpha \equiv r^{-1}\partial_r \Psi_0 \quad \text{and} \quad \beta \equiv r^{-1}\partial_r \Omega_0. \tag{2.8}$$

The full governing equations (2.1), (2.2) have a number of inviscid integral invariants: in particular we consider the enstrophy $E \equiv \int \frac{1}{2}\Omega^2 \,\mathrm{d}\mathbf{r}$, which is conserved for any external forcing of the form (2.3). As discussed more fully in [14], in terms of the weakly nonlinear expansion we can define two contributions to enstrophy at order δ^2, from the mean and azimuthal components,

$$E^{\text{mean}}(t) = \int_0^\infty \Omega_0 \Omega_2 2\pi r \,\mathrm{d}r, \quad E^{\text{azi}}(t) = \int_0^\infty |\omega|^2 2\pi r \,\mathrm{d}r. \tag{2.9}$$

The sum of these two quantities is inviscidly conserved in the weakly nonlinear system and, with suitable initial conditions, for example

$$\Omega_{\text{total}}(r,0) = \Omega_0(r), \qquad \Psi_{\text{total}}(r,0) = \Psi_0(r), \qquad \omega = \psi = \Omega_2 = \Psi_2 = 0, \tag{2.10}$$

the sum $E^{\text{mean}} + E^{\text{azi}}$ is zero for all time. Thus one can study transfers of enstrophy between mean and azimuthal components, as we do below. We shall follow [14] and consider an impulsive external strain field. Imposing a unit impulsive $q(t)$ is equivalent to using the initial condition

$$\omega(r, 0^+) = \mathrm{i}nr^n\beta = \mathrm{i}nr^{n-1}\partial_r\Omega_0 \tag{2.11}$$

for the leading order azimuthal vorticity (from (2.6)) and therefore $E^{\text{azi}} = -E^{\text{mean}}$ is increased to some positive value E_0 at $t = 0^+$. For a Gaussian vortex, as t increases enstrophy is transferred, i.e., rebounds, from the azimuthal to the mean component [12,14]. Eventually E^{azi} and $-E^{\text{mean}}$ both decrease to asymptotic values of about 25% of E_0.

We now extend these results to vortices with sharper edges and introduce the one-parameter family of vortex profiles

$$\Omega_0(r) = \frac{1}{4\pi}\frac{1 - \tanh[(r^2 - \sigma^2)/4(1-\sigma)]}{1 + \tanh[\sigma^2/4(1-\sigma)]}, \tag{2.12}$$

obtained for σ with $0 \leqslant \sigma < 1$ and normalised so $\Omega_0(0) = 1/4\pi$. If $\sigma = 0$ then the vortex has a smooth, broad profile and behaves in a similar manner to the Gaussian vortex while in the limit $\sigma \to 1$ the vortex acquires a top-hat profile with

$$\Omega_0 = 1/4\pi, \quad \alpha = 1/8\pi \quad (r < 1), \qquad \Omega_0 = 0, \quad \alpha = r^{-2}/8\pi \quad (r > 1). \tag{2.13}$$

A code was written (based on NAG routines) to solve the governing system of Eqs. (2.5)–(2.7). With initial conditions given by (2.10), (2.12) the equations can be marched in time for any particular forcing $q(t)$. We have in mind inviscid evolution with $R^{-1} = 0$ in this system, and then the basic vortex Ω_0 remains time-independent in the absence of viscous spreading. However we have to include some viscosity to stabilise the code and the results below were obtained with large R, typically between 10^6 and 10^8. Various values in this range were used in order to confirm the robustness of the results. This, together with the conservation of $E^{\text{mean}} + E^{\text{azi}}$ and the good agreement with inviscid theory given below, indicates that diffusive effects are negligible in the results obtained. Although the aim is to ascertain the evolution of the vortex under an impulsive input, for numerical reasons we set $q(t) = 2T_{\max}^{-1}\sin^2(\pi t/T_{\max})$ for $0 < t < T_{\max}$ and $q(t) = 0$ otherwise. We took $T_{\max} = 1$ which is substantially shorter than other time scales in the problem, with the result is that the forcing is effectively equivalent to an impulsive strain at $t = 0$. The corrections resulting from the finite value of $T_{\max}$ are small, of order at most $\alpha(0)T_{\max} \simeq 4\%$, and we make no further mention of $T_{\max}$.

With the initial conditions (2.10) an impulsive strain field at $t = 0$ generates the non-axisymmetric component ω according to (2.11), and so transfers enstrophy from E^{mean} to E^{azi}, with

$$E^{\text{azi}}(0^+) = -E^{\text{mean}}(0^+) = E_0(\sigma), \tag{2.14}$$

where $E_0(\sigma)$ can be found for the family of profiles by substituting (2.11), (2.12) in E^{azi} (2.9) and computing the integral numerically. The integral is of order $(1-\sigma)^{-1}$ as $\sigma \to 1$, due to the sharpening of the profile.

The question then is: how do $E^{\text{mean}}(t)$ and $E^{\text{azi}}(t)$ evolve at later times for a given vortex profile? To answer this we defined a normalised suppression factor

$$S(t, \sigma) \equiv \frac{E_0(\sigma) - E^{\text{azi}}(t)}{E_0(\sigma)} \tag{2.15}$$

for a given vortex profile parameterised by σ; $S(0^+, \sigma) = 0$ and $S(t, \sigma)$ increases as enstrophy is transferred from azimuthal to mean by the rebound phenomenon. It proved useful to look at an asymptotic suppression factor for the given vortex defined as

$$S_\infty(\sigma) = \lim_{t\to\infty} S(t, \sigma). \tag{2.16}$$

Fig. 1 shows the evolutions of the normalised mean and azimuthal enstrophies as functions of time for different values of σ. The solid line corresponds to $\sigma = 0$, the broadest vortex profile, and this shows the most rapid suppression of azimuthal enstrophy at moderate times $t \leqslant 400$. For large times we obtain $S_\infty \simeq 0.8$ so that about 80% of the enstrophy is transferred back from the fluctuating to the mean component. This is a greater suppression than was observed for the Gaussian vortex [14] when $S_\infty \simeq 0.75$. In Fig. 1 the dotted and dashed lines correspond to increased values of $\sigma = 0.75$ and 0.9 and here we see a slower initial suppression of azimuthal vorticity; however for large times the asymptotic suppression of vorticity becomes greater, with $S_\infty \simeq 0.82$ and 0.93 respectively. In the figure $\sigma = 0.92$ (dash–triple-dot) is also illustrated: E^{azi} is still decreasing at $t = 2000$ and does not saturate until $t = 4000$ (not shown) with $S_\infty \simeq 0.95$. Finally the case $\sigma = 0.95$ has yet slower evolution, but larger values of σ are not accessible by our numerical scheme.

In short, the sharper the vortex profile, the greater the suppression of fluctuating vorticity and so the greater the rebound, but this occurs on a slower and slower time scale. Note that for a top-hat vortex, an impulsive weak strain would render the vortex slightly elliptical and it would then rotate with no transfer of enstrophy back to the mean. (This applies once the vortex

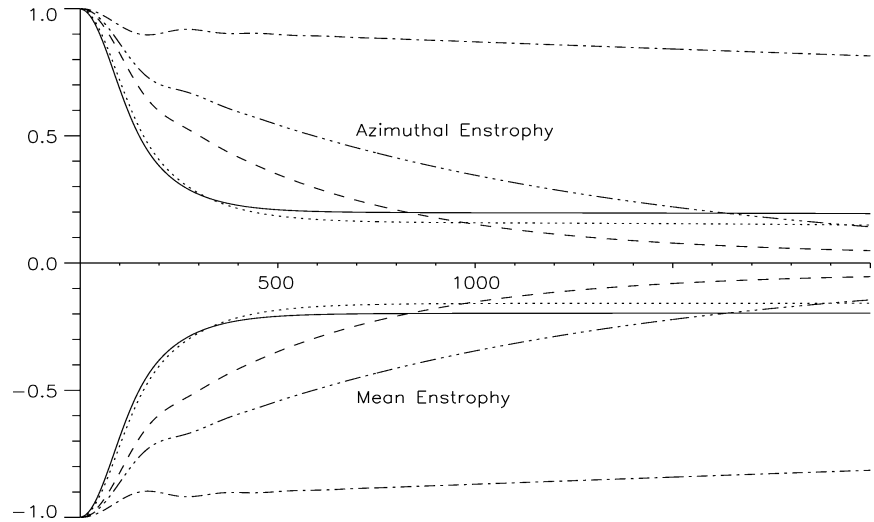

Fig. 1. Evolution of normalised enstrophies $E^{\mathrm{azi}}(t)/E_0(\sigma)$ (top curves) and $E^{\mathrm{mean}}(t)/E_0(\sigma)$ (lower curves) for different values of σ. The horizontal axis shows time linearly from $t = 0$ to 2000. The curves correspond to $\sigma = 0$ (solid), 0.75 (dot), 0.9 (dash), 0.92 (dash–triple-dot) and 0.95 (dash–dot).

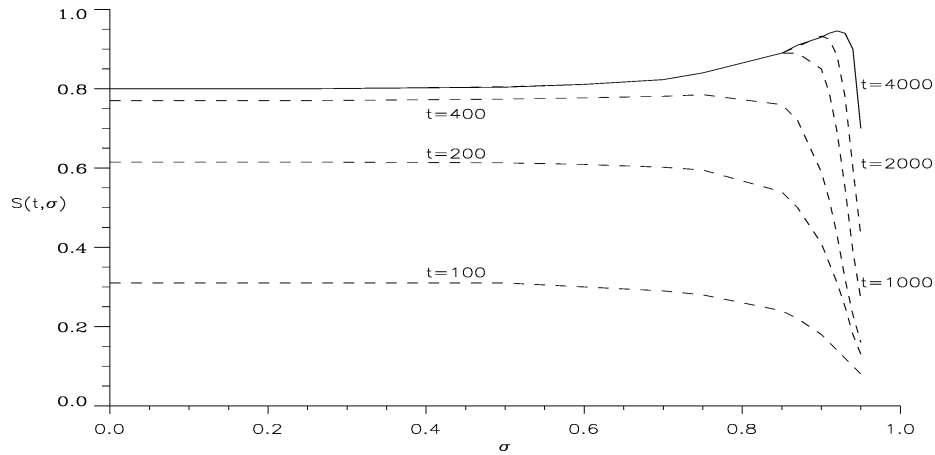

Fig. 2. Suppression of fluctuating enstrophy $S(t, \sigma)$ plotted against σ for $t = 100$, 200, 400, 1000, 2000 and 4000.

is subject to zero background strain: if the straining field were to be maintained the aspect ratio of the vortex would oscillate in time e.g., [20] or [31].) For any *finite* value of time t our results as $\sigma \to 1$ approach this limit in which there is no rebound.

However the *asymptotic* rebound as $t \to \infty$, measured by $S_\infty(\sigma)$, appears to increase to unity as the vortex edge is made sharper $\sigma \to 1$, corresponding to a complete rebound of azimuthal enstrophy. In this sense a sharp-edged yet smooth vortex appears to be more robust than a distributed vortex, as it can axisymmetrise with relatively low loss of enstrophy to azimuthal components; however the process takes longer and longer so, on moderate time-scales, the vortex behaves largely as a top-hat vortex exhibiting a normal mode.

For another view of these results, Fig. 2 shows $S(t, \sigma)$ plotted against σ for given times t. The σ scale thus corresponds to broad vortices on the left which become increasingly sharp as $\sigma \to 1$. For $\sigma < 0.75$ the suppression of vorticity is about $S_\infty(\sigma) \simeq 0.8$ and has largely occurred by $t = 400$. As $\sigma \to 1$, the suppression becomes progressively slower as the individual curves $t = \text{const.}$ head downward; however the asymptotic $t \to \infty$ suppression (see the $t = 4000$ curve) increases and it appears that $S_\infty(\sigma) \to 1$ as $\sigma \to 1$. Note that the above runs were performed with $R = 10^8$ and $E^{\mathrm{azi}} + E^{\mathrm{mean}} = 0$ to within graphical accuracy in Fig. 1. The effects of viscosity are felt first in the azimuthal enstrophy, which is destroyed on a shear–diffuse time-scale of order $R^{1/3}$ [13,32–35]. This is evident in similar runs with $R = 10^6$ but will not be described further here.

3. Compact vortices with skirts and fine-scale structure

In this section we develop the theory of a compact vortex with weak vorticity at its periphery. Our aims are to understand the vorticity suppression and rebound seen for the family of vortices (2.12) studied numerically above, and to extend our study to discuss the effects of fine-scale vorticity. The analysis is closely modelled on BLSY, but includes additional terms to incorporate the effects of fine-scale vorticity.

3.1. Framework

The general configuration we study is shown schematically in Fig. 3. The vorticity is supposed to consist of three components. First there is the vortex $\Omega_{\rm c}$, illustrated here as a top-hat vortex but which can be made more general as long as it has the key property that it is compact and vanishes entirely for $r > r_0$. It is convenient to take the vortex to have positive vorticity, so that the angular velocity is positive and decreases outside the vortex, whereupon

$$\Omega_{\rm c}(r) \geqslant 0 \quad (r < r_0), \qquad \alpha_{\rm c}'(r) < 0 \quad (r > r_0). \tag{3.1}$$

Superimposed on the compact vortex is a 'skirt' $\varepsilon\Omega_{\rm s}$; this is weak vorticity which varies on the same $r = {\rm O}(1)$ length scale as the main vortex itself. The third component $\varepsilon^2\Omega_{\rm L}$ is weaker still and varies on a short length-scale localised in a critical layer, as explained below.

First consider disturbances to the compact vortex alone $\Omega_0 = \Omega_{\rm c}$. Normal mode solutions (if they exist) take the form $\omega = g(r)\,{\rm e}^{-{\rm i}n\varpi t}$, $\psi = f(r)\,{\rm e}^{-{\rm i}n\varpi t}$, where from (2.6), with $R^{-1} = 0$ and $q(t) \equiv 0$, we have

$$\big(\alpha_{\rm c}(r) - \varpi\big)g = \beta(r)f = r^{-1}\Omega_{\rm c}'(r)f, \qquad g = \Delta_1 f; \tag{3.2}$$

here $\alpha_{\rm c}(r)$ is the angular velocity corresponding to the compact vortex $\Omega_{\rm c}(r)$. We *assume* that the compact vortex possesses such a normal mode for some given n. The structure of (3.2) demonstrates that there is a critical radius r_n, defined by $\alpha_{\rm c}(r_n) = \varpi$, corresponding to where the normal mode frequency is equal to the angular frequency of the flow. Let us assume that r_n lies outside the compact vortex ($r_n > r_0$) for otherwise Eq. (3.2) generally develop a singularity at $r = r_n$ [36]. Lastly, in anticipation of the later development, it is convenient to normalise this mode so that $f(r_n) = 1$.

If now additional vorticity is introduced, whether it be the weak skirt $\Omega_{\rm s}$ or fine structure $\Omega_{\rm L}$, what is crucial is its distribution within the critical layer of width ε surrounding the radius $r = r_n$. This will generally lead to damping, destabilisation or oscillations of the normal mode thus generating a 'quasi-mode'. To examine this, it is convenient to take our basic axisymmetric vortex as

$$\Omega_0 = \Omega_{\rm c}(r) + \varepsilon\Omega_{\rm s}(r) + \varepsilon^2\Omega_{\rm L}(Y), \quad Y \equiv \varepsilon^{-1}(r - r_n); \tag{3.3}$$

here $0 < \varepsilon \ll 1$ and Y is an inner variable within the critical layer. It is helpful to suppose that the corresponding vorticity gradient $\Omega_{\rm L}'(Y)$ falls off rapidly as $Y \to \pm\infty$.

The normal mode is coupled to vorticity gradients in the critical layer rather than vorticity itself and the above scaling gives similar gradients for the $\Omega_{\rm s}$ and $\Omega_{\rm L}$ components. However the corresponding angular velocity contributions are different: $\varepsilon\Omega_{\rm s}$ gives rise to an angular velocity $\varepsilon\alpha_{\rm s}$, whereas that for $\varepsilon^2\Omega_{\rm L}$ is at most of order ε^2 and is negligible in the development below. We note that the tanh profiles (2.12) studied above can be fitted into this framework: we take $\Omega_{\rm L} \equiv 0$, $\Omega_{\rm c}$ a top-hat vortex, and $\Omega_{\rm s}$ the exponential tail of the profile, with ε scaled as its magnitude at $r = r_n$.

We seek a solution which at leading order is simply the rotating normal mode, but which evolves on a long time scale $\tau = \varepsilon t$, and set $\omega = \zeta(r,\tau)\,{\rm e}^{-{\rm i}n\varpi t}$ and $\psi = \chi(r,\tau)\,{\rm e}^{-{\rm i}n\varpi t}$. We see that Eqs. (2.6), (2.8) now become

$$\varepsilon\partial_\tau\zeta + {\rm i}n\big(\tilde\alpha_{\rm c} + \varepsilon\alpha_{\rm s} + {\rm O}\big(\varepsilon^2\big)\big)\zeta - {\rm i}nr^{-1}\big(\Omega_{\rm c}' + \varepsilon\Omega_{\rm s}' + \varepsilon\Omega_{\rm L}'\big)\chi = 0 \tag{3.4}$$

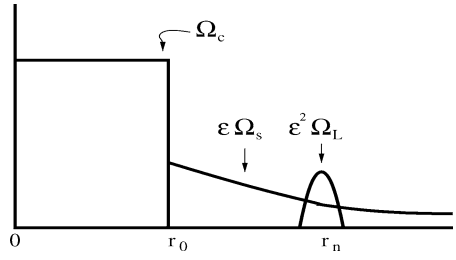

Fig. 3. Schematic diagram of the axisymmetric vorticity profile $\Omega_0(r)$. The compact vortex $\Omega_{\rm c}$ is shown here as a top-hat vortex but may in fact be more general. The skirt vorticity $\varepsilon\Omega_{\rm s}$ varies on scales of order unity, while the fine-scale vorticity $\varepsilon^2\Omega_{\rm L}$ varies on a short length-scale of order ε.

where $\tilde{\alpha}_c(r) = \alpha_c(r) - \varpi \equiv \alpha_c(r) - \alpha_c(r_n)$, $\zeta = \Delta_1 \chi$ and the dashes denote differentiation with respect to variable r or Y as appropriate (see (3.3)).

We expand $\zeta(r,\tau)$ and $\chi(r,\tau)$ in powers of ε, with $\zeta = \zeta_0 + \varepsilon\zeta_1 + O(\varepsilon^2)$ and $\chi = \chi_0 + \varepsilon\chi_1 + O(\varepsilon^2)$. The leading order system for ζ_0 and χ_0 is simply (3.2) with solution

$$\chi_0 = f(r)a(\tau), \qquad \zeta_0 = g(r)a(\tau), \tag{3.5}$$

where we recall that f, g define the normal mode of the compact vortex and $a(\tau)$ is an unknown complex amplitude.

3.2. Outer solution

The normal mode amplitude $a(\tau)$ will be determined from (3.4) at order ε (see BLSY). We first consider this equation for values of r outside the critical layer, that is for $|r - r_n| \gg \varepsilon$; here the fine-scale vorticity gradient $\Omega_L'(Y)$ is negligible, and this leaves

$$\partial_\tau \zeta_0 + \mathrm{i}n(\tilde{\alpha}_c\zeta_1 + \alpha_s\zeta_0) - \mathrm{i}nr^{-1}\big(\Omega_c'\chi_1 + \Omega_s'\chi_0\big) = 0, \qquad \zeta_1 = \Delta_1\chi_1. \tag{3.6}$$

These are equations for ζ_1 and χ_1, and (using (3.5)) may be combined as

$$\mathrm{i}n\big(\Delta_1 - \tilde{\alpha}_c^{-1}r^{-1}\Omega_c'\big)\chi_1 = \tilde{\alpha}_c^{-1}\big(-g\partial_\tau a - \mathrm{i}n\alpha_s g a + \mathrm{i}nr^{-1}\Omega_s' f a\big). \tag{3.7}$$

As the critical layer $r \simeq r_n$ is approached so $\tilde{\alpha}_c$ tends to zero; however both Ω_c and g (from (3.2)) are identically zero outside the compact vortex, and so the only singular term present is $\tilde{\alpha}_c^{-1}\mathrm{i}nr^{-1}\Omega_s' f a$ on the right-hand side, which gives a simple pole singularity. The equation may be written in the form [16],

$$\big(\Delta_1 - \tilde{\alpha}_c^{-1}r^{-1}\Omega_c'\big)\chi_1 = \mu a(\tau) f(r)(r - r_n)^{-1} + R(r), \quad \mu = \Omega_s'(r_n)/r_n\alpha_c'(r_n), \tag{3.8}$$

where the remaining terms are bundled into $R(r)$, which is non-singular as the critical radius is approached. (Note that $\tilde{\alpha}_c'(r) \equiv \alpha_c'(r)$.)

There is a corresponding singularity in the stream function χ_1, which takes the form

$$\chi_1(r,\tau) \simeq \chi_1(r_n,\tau) + \mu a(\tau)(r - r_n)\log|r - r_n| + (r - r_n)\begin{cases} c^-(\tau) & (r < r_n), \\ c^+(\tau) & (r > r_n) \end{cases} \tag{3.9}$$

(using the normalisation condition $f(r_n) = 1$). The jump in derivative is related to the behaviour inside the critical layer which we will analyse shortly. Integrating Eq. (3.8) for $r < r_n$ and $r > r_n$ yields an equation for $a(\tau)$. This procedure is explained in BLSY and we give only the result,

$$c^+ - c^- = \mathrm{i}I_1\partial_\tau a + (I_2 + I_3 + I_4)a. \tag{3.10}$$

Here I_1 (>0), I_2, I_3 and I_4 are constants which are defined in terms of integrals involving f and g that depend only on the structure of the original compact vortex.

3.3. Inner solution and coupled system

The solution for the stream function χ in the critical layer, defined by $Y \equiv \varepsilon^{-1}(r - r_n) = O(1)$, must match onto the singularity identified above in (3.9). It may be written as a Taylor expansion of the outer components χ_0, χ_1 discussed above, plus an additional term $\Phi(Y,\tau)$ so that

$$\begin{aligned}\chi(r,\tau) \;=\; &\big[\chi_0(r_n,\tau) + \varepsilon Y\partial_r\chi_0(r_n,\tau) + \tfrac{1}{2}\varepsilon^2 Y^2\partial_r^2\chi_0(r_n,\tau)\big] \\ &+ \big[\varepsilon\chi_1(r_n,\tau) + \varepsilon^2 a\mu Y\log\varepsilon + \varepsilon^2\Phi(Y,\tau)\big] + \varepsilon^2\chi_2(r_n,\tau) + o\big(\varepsilon^2\big)\end{aligned} \tag{3.11}$$

which acquires the singular behaviour in (3.9),

$$\Phi \sim \mu a Y\log|Y| + Yc^\pm, \quad \Phi_Y \sim \mu a\log|Y| + \mu a + c^\pm \quad (Y \to \pm\infty). \tag{3.12}$$

From this we obtain the jump in gradient across the critical layer as the principal value integral

$$c^+(\tau) - c^-(\tau) = \lim_{Y\to\infty}\big[\Phi_Y(Y,\tau)\big]_{-Y}^{Y} = \lim_{Y\to\infty}\int_{-Y}^{Y}\Phi_{YY}(Y,\tau)\,\mathrm{d}Y; \tag{3.13}$$

this quantity may be identified with the 'phase shift' which plays a key role in critical layer theory (e.g., [37]).

In the critical layer, the vorticity equation (3.4) becomes at leading order (with $\chi \simeq f(r_n)a(\tau) = a(\tau)$)

$$\partial_\tau \zeta + \mathrm{i}n(\alpha_\mathrm{s}(r_n) + Y\alpha_c'(r_n))\zeta - \mathrm{i}nr_n^{-1}\big[\Omega_\mathrm{s}'(r_n) + \Omega_\mathrm{L}'(Y)\big]a = 0. \tag{3.14}$$

Note that the fine-scale vorticity gradient Ω_L' makes an appearance here as a Y-dependent term in the equation.

From $\zeta = \Delta_1\chi$ applied to the expansion (3.11) we also deduce that $\zeta \simeq \Phi_{YY}$ at leading order gives the vorticity in the critical layer. Combining this, (3.10) and (3.13) yield

$$\mathrm{i}I_1\partial_\tau a + (I_2 + I_3 + I_4)a = \lim_{Y\to\infty} \int_{-Y}^{Y} \zeta(Y,\tau)\,\mathrm{d}Y \tag{3.15}$$

and the two equations (3.14), (3.15) constitute a partial differential equation for the critical layer vorticity $\zeta(Y,\tau)$, coupled to an ordinary differential equation for the quasi-mode amplitude $a(\tau)$. All other quantities are given in terms of the structure of the basic axisymmetric vortex.

3.4. Numerical results for $\Omega_\mathrm{L} \equiv 0$

We will consider two situations, $\Omega_\mathrm{L}(Y) = 0$ in this section, and $\Omega_\mathrm{s}(r) = 0$ in the next. If $\Omega_\mathrm{L}(Y) = 0$ there is no fine structure and simply a smooth skirt around the vortex; it then makes sense to non-dimensionalise using μ in (3.8), that is to base scales on the key quantity of the vorticity gradient in the skirt at the critical layer, $\Omega_\mathrm{s}'(r_n)$ [16]. We set $\mathcal{L} = -|\mu|/I_1\alpha_\mathrm{c}'(r_n) > 0$, $\mathcal{T} = I_1/|\mu| > 0$ and $\varsigma = -\mathcal{T}(I_2 + I_3 + I_4)/I_1$. Recycling earlier notation, we then define a time coordinate t and a space coordinate y, given by $\mathcal{T}t = \tau$, $\mathcal{L}(y - \varsigma/n)\alpha_\mathrm{c}'(r_n) = (\alpha_\mathrm{s}(r_n) + Y\alpha_\mathrm{c}'(r_n))$, together with rescaled quasi-mode amplitude $\eta(t) = (\mathcal{T}/r_n\mathcal{L})a(\tau)\,\mathrm{e}^{\mathrm{i}\varsigma t}$ and vorticity $\hat{\zeta} = (\mathcal{T}/r_n|\mu|)\zeta\,\mathrm{e}^{\mathrm{i}\varsigma t}$. Note that our choice of y has the opposite sign to that in BLSY as we wish to retain y as a surrogate radial coordinate, with y increasing radially outwards.

With these rescalings (and dropping the hat from $\hat{\zeta}$) we obtain

$$\partial_t\zeta - \mathrm{i}ny\zeta - \mathrm{i}n\lambda\eta = 0, \qquad \mathrm{i}\partial_t\eta = \int_{-\infty}^{\infty} \zeta\,\mathrm{d}y, \tag{3.16}$$

where $\lambda = \pm 1$ gives the sign of the vorticity gradient $\Omega_\mathrm{s}'(r_n)$ in the critical layer, defined by

$$\lambda = -\frac{\mu}{|\mu|} = -\operatorname{sign}\mu = \operatorname{sign}\Omega_\mathrm{s}'(r_n) \tag{3.17}$$

(bearing in mind (3.1) and (3.8b)). A principal value integral is assumed in (3.16b) (cf. (3.15)) and in similar contexts below.

For the system (3.16) we use the initial conditions

$$\zeta(y,0) = 0, \qquad \eta(0) = 1, \tag{3.18}$$

corresponding to excitation of the normal mode only at $t = 0$. In Section 5 below we use these initial conditions to solve for the case where there is fine structure in the vortex. Here though the system (3.16) reduces to the ordinary differential problem $\partial_t\eta = \pi\lambda\eta$ with solution [16]

$$\eta = \mathrm{e}^{\gamma t}, \quad \gamma = \pi\lambda. \tag{3.19}$$

If $\lambda = 1$ then the vorticity gradient in the skirt is positive and the normal mode is destabilised, but if $\lambda = -1$ then the mode is stable. As discussed in BLSY the combination of the normal mode, amplitude $a(\tau)$ and the winding-up of vorticity $\zeta(y,\tau)$ in the critical layer constitutes the quasi-mode.

For our purposes we wish to compare the growth rate γ with our numerical results for enstrophy rebound. Returning to our original units, γ becomes

$$\gamma_* = \pi\lambda\varepsilon/\mathcal{T} = -\varepsilon\pi\,\Omega_\mathrm{s}'(r_n)/r_n\alpha_\mathrm{c}'(r_n)I_1 \tag{3.20}$$

and so for a top-hat vortex with $n = 2$, $r_2 = \sqrt{2}$, we have $\alpha_\mathrm{c}'(r_2) = -(8\pi\sqrt{2})^{-1}$ and $I_1 = 64\pi\sqrt{2}$ whence

$$\gamma_* = \frac{\pi\varepsilon\Omega_\mathrm{s}'(\sqrt{2})}{8\sqrt{2}}. \tag{3.21}$$

We now apply this growth rate (3.21) to the family of vortices introduced in (2.12), in the limit $\sigma \to 1$, when the vortex has a sharp edge at $r = 1$, of width order $(1-\sigma)^{-1}$, and an exponentially decaying tail of vorticity for $r > 1$. We take the compact vortex $\Omega_\mathrm{c}(r)$ to be simply the top-hat vortex, with the skirt consisting of the exponential tail of the tanh function. The key quantity in the above analysis is $\varepsilon\Omega_\mathrm{s}'(\sqrt{2})$ which we equate to $\Omega_0'(\sqrt{2})$ (from (2.12)) to give $\gamma_* = \pi\,\Omega_0'(\sqrt{2})/8\sqrt{2}$.

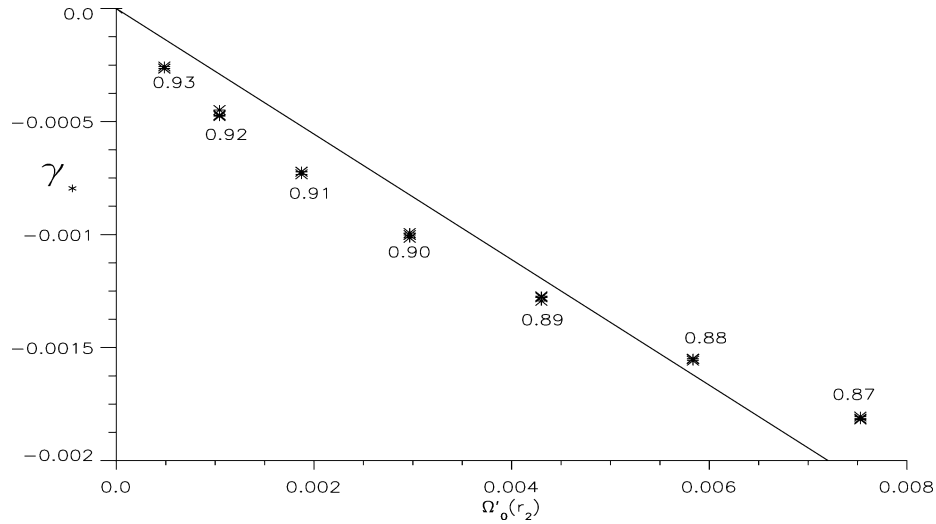

Fig. 4. Exponential growth rates γ_* plotted against $\Omega'_0(r_2)$, $r_2 = \sqrt{2}$. The asterisks show numerically measured growth rates for values of $0.87 < \sigma < 0.93$ obtained by solving (2.6) with profiles (2.12), whilst the solid line represents the asymptotic solution (3.21).

This approximate negative growth rate is plotted as a solid straight line in Fig. 4 as γ_* against $\Omega'_0(\sqrt{2})$. Data points show the decay rate of azimuthal enstrophy for different values of σ from 0.87 to 0.93. These points were obtained by solving the partial differential equation (2.6) numerically for the profile (2.12) and initial conditions (2.10). The decay rates were measured from the formula for $\partial_t E^{\mathrm{azi}}$,

$$\partial_t E^{\mathrm{azi}}(t) = \mathrm{i}n \int_0^\infty \beta(r)(\omega^* \psi - \omega \psi^*) 2\pi r \, \mathrm{d}r, \tag{3.22}$$

obtained from (2.6), (2.9) with $q \equiv 0$ and $R^{-1} = 0$. The right-hand side was computed numerically and fitted to the decay law $\partial_t E^{\mathrm{azi}} \propto \mathrm{e}^{2\gamma t}$ to obtain $\gamma(\sigma)$ from each numerical run.

There is a reasonable numerical agreement between data points (asterisks) and the approximate theory in Fig. 4, suggesting that the rebound phenomenon is indeed linked to the decay of a quasi-mode in the sharp-edged vortex. The agreement begins to break down for $\sigma < 0.87$, when the vortex edge is too broad for the asymptotic theory to be valid. For $\sigma \gtrsim 0.93$, the timescale required to derive the numerical decay rate is so long that viscosity is influencing the results.

The quasi-mode and critical layer vorticity may be observed in our numerical simulations. From $\omega(r, t)$ we may reconstruct the evolution of linear perturbations to the vortex from Eq. (2.4) and in Fig. 5 we show $\omega(r, t)\,\mathrm{e}^{\mathrm{i}n\theta} + \text{c.c.}$ as a grey-scale plot for various times with $\sigma = 0.75$ (left panels) and $\sigma = 0.9$ (right panels). In both cases the initial impulsive kick excites a four-lobed vorticity distribution with $n = 2$ (top left and right). In the evolution with $\sigma = 0.75$ this leads to spiral wind-up of vorticity fluctuations. By $t = 2001$ we see faint evidence of a quasi-mode, and we also see the diffusive decay examined in [32]. When $\sigma = 0.9$ note that initially the four-lobed structure is more tightly localised around the sharp vortex edge at $r = 1$. As the vorticity evolves this four-lobed structure maintains its integrity: it is essentially the normal mode of the top hat vortex. However spiral wind-up of fluctuations is occurring further out and this leads to the damping of the normal mode. The coupled system of damped normal mode and spiral wind-up in the critical layer constitutes the quasi-mode discussed above.

Fig. 6 shows the physical mechanism by which the normal mode component of the quasi-mode is damped in the case when the vorticity gradient is negative in the critical layer. In (a) the thicker, inner circle shows the compact vortex (of positive vorticity), say a top-hat vortex, while the thinner, outer circle denotes the critical layer containing weak, smooth vorticity. An $n = 2$ normal mode is generated by a straining distortion. This leads to a distorted compact vortex shown in (b), and so enhanced and decreased vorticity shown by $+$ and $-$. This generates a secondary flow, shown by arrows. This secondary flow affects the vorticity in the critical layer, and with a negative vorticity gradient generates enhanced and decreased vorticity as shown in (c). The flow resulting from the vorticity in the critical layer depicted in (c) acts to counteract the original distortion in (a). The net effect is to stabilise the normal mode; in the case of positive vorticity gradient in the critical layer the effect would be destabilising. Note that this explanation is somewhat simplified as it neglects the spiral wind-up that is occurring in the critical layer, leading to the integro-differential system (3.16).

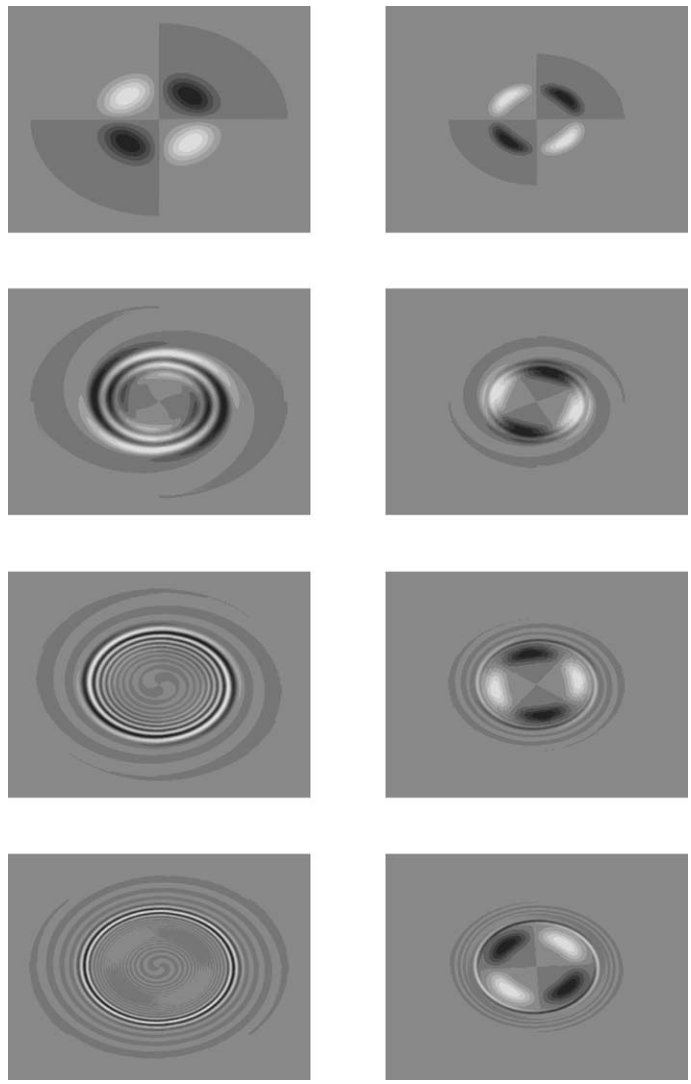

Fig. 5. Contour plot of linear vorticity evolution subject to weak viscosity, $R = 10^8$, for $n = 2$ with $\sigma = 0.75$ (left panels) and $\sigma = 0.9$ (right panels). The x and y axes range from $-\pi$ to π. Reading downwards on each side we have plots at times $t = 1$, $t = 201$, $t = 1001$ and $t = 2001$.

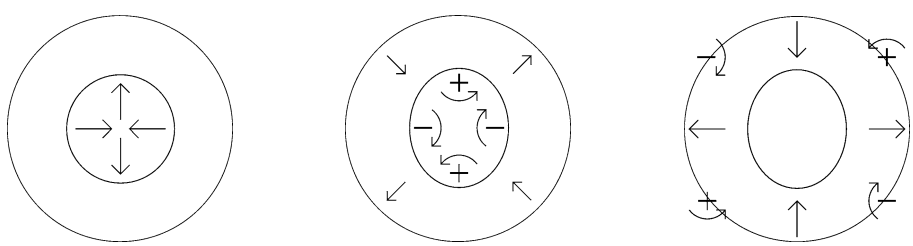

Fig. 6. Physical mechanism for quasi-mode damping. See discussion in the text.

4. Effect of fine-scale vorticity in the critical layer

We have studied the case above of a compact vortex surrounded by a skirt of weak vorticity; in the skirt, the vorticity has gradients of magnitude ε. We now allow the vorticity to vary on a finer scale, and to isolate its effects we set $\Omega_{\rm S}(r) \equiv 0$ but allow $\Omega_{\rm L}(Y)$ to be non-zero. Recalling Eq. (3.3), the full vorticity distribution is now $\Omega_0 = \Omega_{\rm c}(r) + \varepsilon^2\Omega_{\rm L}(Y)$ where $Y = \varepsilon^{-1}(r - r_n)$. The vorticity gradients in the critical layer are again of order ε, and couple to the evolution of the normal mode amplitude to give a system possessing a quasi-mode, as we shall see below. In this case the gradient of vorticity in the critical layer is not constant and so formula (3.21) for the quasi-mode decay rate requires modification.

We therefore return to the coupled system of the PDE (3.14) for critical layer vorticity $\zeta(\tau, Y)$, and the ODE (3.15) for the quasi-mode amplitude $a(\tau)$. We delete the skirt vorticity, $\Omega_{\rm S}(r) = 0$ and $\alpha_{\rm S}(r) = 0$, and note that consequently $\mu = I_2 = I_3 = I_4 = 0$ (see [16]). This leaves

$$\partial_\tau\zeta + {\rm i}nY\alpha_{\rm c}'(r_n)\zeta - {\rm i}nr_n^{-1}\Omega_{\rm L}'(Y)a = 0, \qquad {\rm i}I_1\partial_\tau a = \int_{-\infty}^{\infty} \zeta(Y,\tau)\,{\rm d}Y. \tag{4.1}$$

Now that we have suppressed the skirt we need to adapt the details of the non-dimensionalisation to be applied to the system (4.1). This is based on the maximum gradient of $\Omega_{\rm L}(Y)$ in the critical layer and we set

$$\mu_{\rm L} = \Omega_{\rm Lmax}'/r_n\alpha_{\rm c}'(r_n) < 0, \quad \Omega_{\rm Lmax}' = \max_Y\big|\Omega_{\rm L}'(Y)\big| > 0, \tag{4.2}$$

$$\mathcal{L} = -|\mu_{\rm L}|/I_1\alpha_{\rm c}'(r_n) > 0, \quad \mathcal{T} = I_1/|\mu_{\rm L}| > 0 \tag{4.3}$$

(bear in mind that $\alpha_{\rm c}'(r_n) < 0$ from (3.1) and I_1 is positive [16]). Replacing

$$\mathcal{T}t = \tau, \quad \mathcal{L}y = Y, \quad \eta(t) = (\mathcal{T}/r_n\mathcal{L})a(\tau), \quad \hat{\zeta} = \big(\mathcal{T}/r_n|\mu_{\rm L}|\big)\zeta, \tag{4.4}$$

in (4.1) and dropping the hat on $\hat{\zeta}$ gives a coupled system

$$\partial_t\zeta - {\rm i}ny\zeta - {\rm i}n\lambda(y)\eta = 0, \qquad {\rm i}\partial_t\eta(t) = \int_{-\infty}^{\infty} \zeta(y,t)\,{\rm d}y. \tag{4.5}$$

Now λ is a function of y given by

$$\lambda(y) = \Omega_{\rm L}'(Y)/\Omega_{\rm Lmax}' \qquad (\mathcal{L}y = Y) \tag{4.6}$$

and is the vorticity gradient of the critical layer vorticity, normalised to have maximum modulus unity. In the case where the vorticity gradient is a constant we recover the previous definition (3.17). We remark that in developing the above theory we have assumed that the vorticity gradient $\Omega_{\rm L}'(Y)$ is localised in the skirt, falling off rapidly as $Y \to \pm\infty$ which allows the vorticity itself to tend to (possibly different) constants as $Y \to \pm\infty$.

In view of the various changes of variables it is worth recording that a growth rate γ and the spatial variable y in the present rescaled system are related to a growth rate γ_* and the variable r in the original system by

$$\gamma_* = \varepsilon\gamma/\mathcal{T} = \big(-\varepsilon\Omega_{\rm Lmax}'/r_nI_1\alpha_{\rm c}'\big)\gamma, \qquad r - r_n = \varepsilon\mathcal{L}y = \big(\varepsilon\Omega_{\rm Lmax}'/r_nI_1\alpha_{\rm c}'^2\big)y. \tag{4.7}$$

We will shortly consider a number of illustrative profiles for $\Omega_{\rm L}(Y)$ and so $\lambda(y)$, and these are shown schematically in Fig. 7. We recall from the introduction that vortex stripping, collisions and axisymmetrization processes often lead to a vortex with a ring of vorticity at its periphery [26]. We first of all idealise such a vortex as axisymmetric (although, in practice, superposed will be non-axisymmetric fluctuations undergoing spiral wind-up). Crucial then is the distribution of vorticity in the critical layer $r \simeq r_n$. Representative cases to consider are when the vorticity distribution has a step-change in the critical layer, which we refer to as an 'up-step' or 'down-step', this could correspond to the edge of a ring of vorticity at the critical layer. A second pair of cases could occur when there is a ring of vorticity of either sign contained within the critical layer leading to a 'bump' or 'trough' in the vorticity distribution. These profiles are illustrated schematically in Fig. 7: along the top row (a), (c), (e), (g) we have $\Omega_{\rm L}(Y)$ representing an up-step, down-step, bump and trough respectively, and underneath in (b), (d), (f), (h) are the corresponding scaled vorticity derivatives $\lambda(y)$, defined in (4.14) below.

To fix ideas let us return to (3.3) and consider profiles of the specific forms

$$\Omega_0(r) = \Omega_{\rm c}(r) \pm \varepsilon^2 w\,{\rm erf}\big((r - r_n)/\varepsilon w\big) \quad \text{(up/down)}. \tag{4.8}$$

The upper sign represents an up-step in the vorticity profile at the critical layer, and the lower sign a down-step. As ever ε is small, and now $w = {\rm O}(1)$ is a parameter that tunes the width and height of the step. Plainly then

$$\Omega_{\rm L}(Y) = \pm w\,{\rm erf}(Y/w), \quad \Omega_{\rm L}'(Y) = \pm 2\pi^{-1/2}\,{\rm e}^{-Y^2/w^2}, \quad \Omega_{\rm Lmax}' = 2\pi^{-1/2}. \tag{4.9}$$

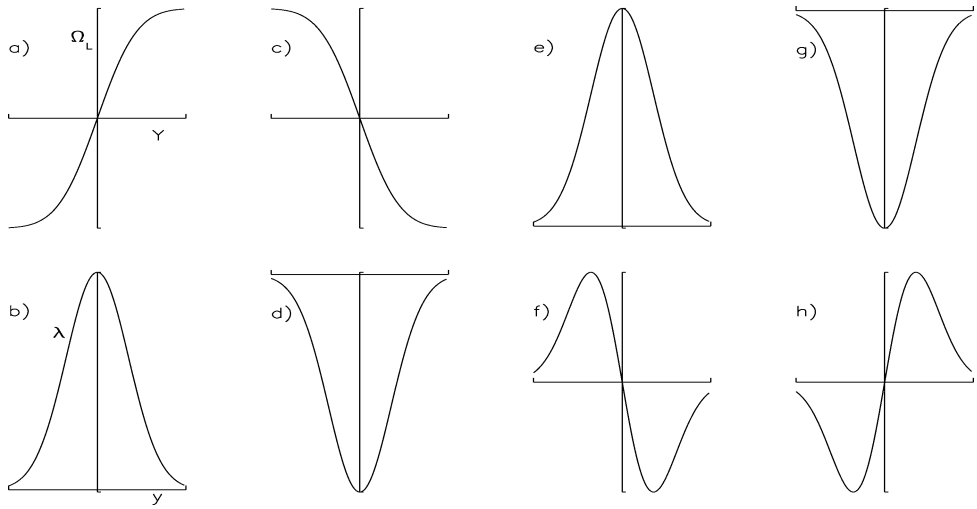

Fig. 7. Schematic picture of the relationship between λ and the shape of vorticity in the critical layer. Top row (a), (c), (e), (g) shows the structure of $\Omega_{\mathrm{L}}(Y)$ whilst the bottom row (b), (d), (f), (h) shows the corresponding $\lambda(y)$. The first column shows the up-step, the second shows the down-step, the third shows a bump and finally the fourth shows a trough.

This now fixes μ_{L} from (4.2) and so $\mathcal{L}$ and $\mathcal{T}$ from (4.3). Finally we may define $\lambda(y)$ from (4.6)

$$\lambda(y) = \pm \mathrm{e}^{-Y^2/w^2} = \pm \mathrm{e}^{-y^2/\kappa^2} \quad (\kappa = w/\mathcal{L}) \tag{4.10}$$

with κ a parameter, proportional to w. (Note that an arbitrary constant can be added on to $\Omega_{\mathrm{L}}(Y)$ without affecting $\lambda(y)$ or subsequent results.)

The other profiles we will consider are

$$\Omega_0(r) = \Omega_{\mathrm{c}}(r) \pm \varepsilon^2 w\, \mathrm{e}^{-(r-r_n)^2/\varepsilon^2 w^2} \quad \text{(bump/trough)} \tag{4.11}$$

where the upper sign represents a bump in the vorticity profile at the critical layer and the lower sign a trough. This gives as above

$$\Omega_{\mathrm{L}}(Y) = \pm w\, \mathrm{e}^{-Y^2/w^2}, \quad \Omega'_{\mathrm{L}}(Y) = \mp 2(Y/w)\, \mathrm{e}^{-Y^2/w^2}, \quad \Omega'_{\mathrm{Lmax}} = (2/\mathrm{e})^{1/2}, \tag{4.12}$$

which determines μ_{L}, $\mathcal{L}$ and $\mathcal{T}$, and then

$$\lambda(y) = \mp(2\,\mathrm{e})^{1/2}(Y/w)\, \mathrm{e}^{-Y^2/w^2} = \mp(2\,\mathrm{e})^{1/2}(y/\kappa)\, \mathrm{e}^{-y^2/\kappa^2} \quad (\kappa = w/\mathcal{L}). \tag{4.13}$$

To summarise and label these different cases, we then have the functions $\lambda(y)$ given by

$$\lambda_1^{\pm}(y) = \pm \mathrm{e}^{-y^2/\kappa^2} \quad \text{(up/down)}, \quad \lambda_2^{\pm}(y) = \mp(2\,\mathrm{e})^{1/2}(y/\kappa)\, \mathrm{e}^{-y^2/\kappa^2} \quad \text{(bump/trough)}. \tag{4.14}$$

We will also examine the effect of shifting the steps $\lambda_1^{\pm}$ within the critical layer, in which y/κ above is replaced by $y/\kappa - \beta$.

5. Numerical methods and results

For a given vorticity profile there are a number of ways to pursue solutions of the coupled system (4.5) subject to the initial condition (3.18). One possibility is to solve the coupled system numerically using a NAG library routine (for example, D03PKF). The disadvantage of this is that weak viscosity must be introduced to avoid the code attempting to trace finer and finer structure in the vorticity field ζ. Alternatively one may solve for ζ in (4.5a) in the form

$$\zeta(y,t) = \mathrm{i}n\lambda(y) \int_0^t \mathrm{e}^{\mathrm{i}ny(t-s)} \eta(s)\, \mathrm{d}s, \tag{5.1}$$

using the initial conditions (3.18), and then substitute into (4.5b) to obtain

$$\partial_t \eta(t) = \int_0^t K(t-s)\eta(s)\,\mathrm{d}s, \quad K(t) = \int_{-\infty}^{\infty} n\lambda(y)\,\mathrm{e}^{\mathrm{i}nyt}\,\mathrm{d}y. \tag{5.2}$$

If this equation is integrated from 0 to t we obtain

$$\eta(t) = 1 + \int_0^t L(t-s)\eta(s)\,\mathrm{d}s, \quad L(t) = \int_0^t K(s)\,\mathrm{d}s. \tag{5.3}$$

The kernel $L(t)$ may be found analytically or numerically and the integral equation (5.3) then passed to a numerical package.

A third approach yields a dispersion relation directly. In simulating the above systems, after a transient we observe exponential behaviour for $\eta(t)$ as $t \to \infty$, and so we may make the *ansatz* $\eta(t) \propto \mathrm{e}^{\gamma t}$ where γ is the complex growth rate. Provided the kernel $K(t-s)$ falls off rapidly (faster than exponentially) with increasing $t-s$, which is the case for the examples given, we may replace the limit 0 in (5.2) by $-\infty$ (valid after any transient) to obtain

$$\gamma = \int_0^{\infty} \mathrm{e}^{-\gamma t} K(t)\,\mathrm{d}t. \tag{5.4}$$

These three methods, based on (4.5), (5.3), (5.4) were all coded and run. All gave consistent results, as a useful check, and also confirmed that the results shown below are effectively inviscid, even when weak viscosity is used to stabilise the code in the case of (4.5). Note that in terms of the original formulation of the problem the growth rate γ_* is related to our non-dimensional growth rate γ by

$$\gamma_* = \frac{\varepsilon\gamma}{r_n|\alpha_{\mathrm{c}}'(r_n)|I_1} \max_Y \left|\Omega_{\mathrm{L}}'(Y)\right| \tag{5.5}$$

(cf. (3.20)) and so is proportional to the maximum vorticity gradient in the critical layer (see (3.3)).

5.1. Steps: up and down

We now consider a number of profiles of $\lambda(y)$, beginning with $\lambda_1^+(y)$ and $\lambda_1^-(y)$ from (4.14), corresponding to an up-step or down-step respectively in the critical layer (see Fig. 7(a)–(d)). Recall that the parameter κ sets the scale of the step and also notice that $\eta(t)$ remains real for all time: this follows from (5.2), since $\lambda(y)$ is an even function and so $K(t)$ is real.

Numerical results for the down-step profile λ_1^- are shown in Fig. 8. The dotted curve shows $\eta(t)$ for $\kappa = 100$, which is the situation in which the vorticity gradient is λ_1^- is of large scale and essentially unity across the critical layer. In this case we

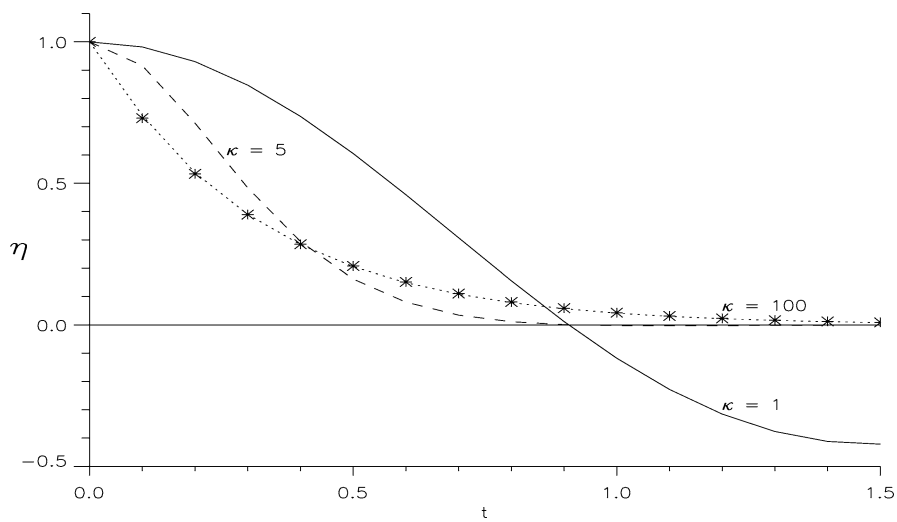

Fig. 8. Numerical behaviour of η plotted against time for a down-step profile $\lambda_1^-(y)$ with $\kappa = 1$ (solid), $\kappa = 5$ (dashed) and $\kappa = 100$ (dotted). The large-κ decay (3.19) is shown with asterisks.

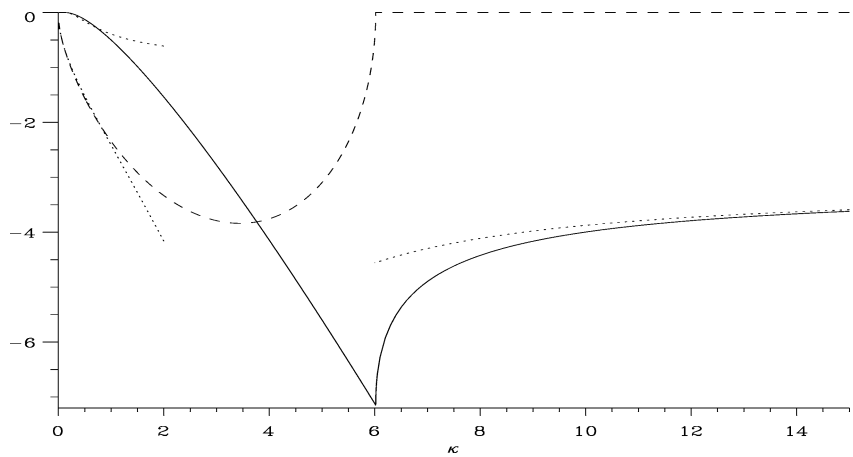

Fig. 9. Plot of $\mathrm{Re}\,\gamma$ (solid) and $\mathrm{Im}\,\gamma$ (dashed) as functions of κ for the down-step profile (4.14a). Dotted lines show the asymptotic results (5.8), (5.10), (5.11) for large κ and small κ. Note that for $\kappa < \kappa_c \simeq 6.018$ there is a complex conjugate pair of modes: only the negative frequencies $\mathrm{Im}\,\gamma$ are shown (i.e., $\mathrm{Im}\,\gamma < 0$).

expect to recover the the decay rate (3.19) derived for a constant gradient, and shown by asterisks – the agreement is excellent. As κ is reduced, the decay at early times becomes weaker, but the final decay becomes stronger as is evident for $\kappa = 5$. As the scale of the down-step κ is further reduced $\eta(t)$ overshoots, and the exponential decay turns into decay with oscillations, as can be seen beginning to happen for $\kappa = 1$ in the figure.

Using the dispersion relation (5.4) the growth rate γ may be found more directly as a function of κ. The kernel $K(t)$ is easily computed from (5.2) and is

$$K(t) = \pm n\kappa\sqrt{\pi}\,\mathrm{e}^{-n^2\kappa^2 t^2/4} \quad \text{(up/down)} \tag{5.6}$$

for the up-step (+ sign) or down-step (− sign). Substituting into (5.4) gives

$$\gamma = \pm\pi\,\mathrm{erfc}(\gamma/n\kappa)\,\mathrm{e}^{\gamma^2/n^2\kappa^2} \quad \text{(up/down)}, \tag{5.7}$$

which may be solved numerically to find γ as a function of the step width κ.

Fig. 9 shows the real and imaginary parts of the growth rate γ for a down-step determined by solving (5.7) with $n = 2$. For $\kappa > \kappa_c \simeq 6.018$ the growth rate is purely real which corresponds to exponential decay. At κ_c the root collides with another real root (corresponding to even stronger decay) and we gain complex conjugate roots for $\kappa < \kappa_c$. As κ is further reduced, the decay rate and frequency decrease. For small κ, the decay is very weak, and the behaviour of the quasi-mode almost purely oscillatory. Note that $\eta(t)$ is purely real in this example, so oscillations do not simply correspond to a changed frequency of rotation of the quasi-mode, but to its amplitude decreasing and increasing, being zero at certain times (as for example at $t \simeq 0.92$ for $\kappa = 1$ in Fig. 8). Fig. 10 shows results for the up-step profile – now the quasi-mode is always unstable with a growth rate γ that is real and increasing with κ.

The dispersion relation (5.7) may be used to glean results valid for large and small κ. With $n = 2$ and $\kappa \gg 1$ then

$$\gamma = \pm\pi - \pi^{3/2}\kappa^{-1} \pm \left(\pi^2 + \pi^3/4\right)\kappa^{-2} + \mathrm{O}\left(\kappa^{-3}\right) \quad \text{(up/down)} \tag{5.8}$$

and as $\kappa \to \infty$ the vorticity gradient becomes constant in the critical layer thereby recovering result (3.19). Figs. 9 and 10 show good agreement between (5.8) and the numerical results.

In the opposite limit with $\kappa \ll 1$ we may use standard formulae (see Chapter 7 of [38]) to give, for an up-step,

$$\gamma = c\kappa^{1/2} + c^{-1}\kappa^{3/2} + \mathrm{O}\left(\kappa^{5/2}\right) \quad \left(c \equiv \sqrt{2}\,\pi^{1/4}\right) \tag{5.9}$$

leading to exponential growth as depicted in Fig. 10. In the case of the down-step we find a similar result

$$\gamma = \pm\mathrm{i}c\kappa^{1/2} \pm \mathrm{i}c^{-1}\kappa^{3/2} \pm \mathrm{O}\left(\kappa^{5/2}\right) \tag{5.10}$$

and we note that (5.10) appears to predict purely imaginary solutions for small κ. This is so to all algebraic powers of κ but there is also a weak decay given by

$$\mathrm{Re}\,\gamma \simeq -\left(\pi/2\sqrt{\mathrm{e}}\right)\mathrm{e}^{-\sqrt{\pi}/n\kappa}. \tag{5.11}$$

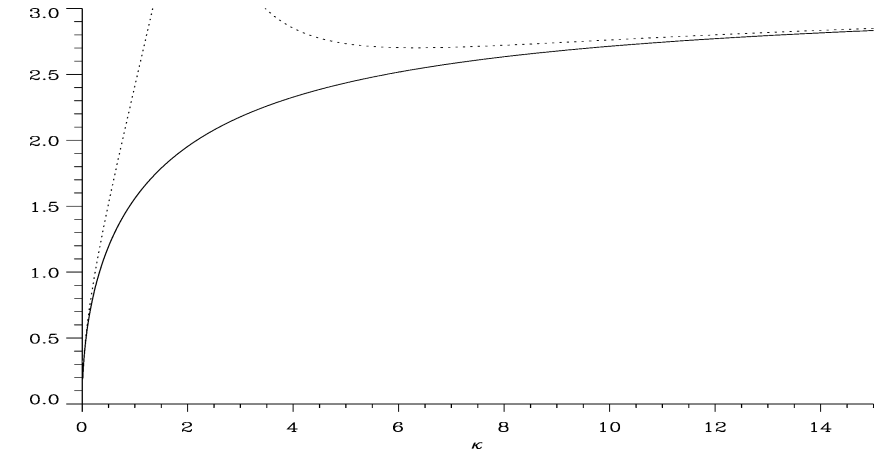

Fig. 10. Plot of the real growth rate γ (solid) as a function of κ for the up-step profile (4.14a). Dotted lines show the asymptotic results (5.8), (5.9) for small κ and large κ.

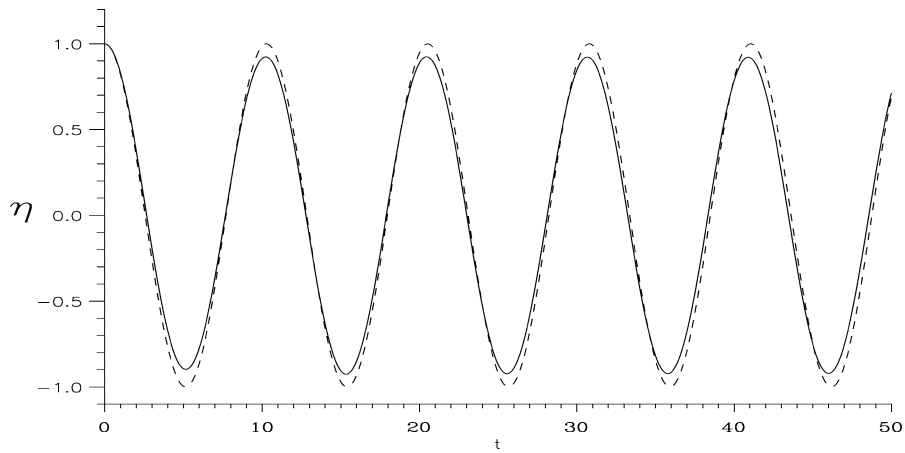

Fig. 11. Behaviour of $\eta(t)$ for a narrow down-step, $\lambda_1^-(y)$, with $\kappa = 0.1$. We show numerical results (solid) and the asymptotic approximation (dashed) $\eta \approx \cos[(c\kappa^{1/2} + c^{-1}\kappa^{3/2})t]$, $c \equiv \sqrt{2}\,\pi^{1/4}$, derived using (5.10).

The oscillatory behaviour of the amplitude $\eta(t)$ for a narrow down-step with $\kappa = 0.1$ is shown in Fig. 11. Fig. 12 shows the corresponding vorticity field in the critical layer at times corresponding to minima or maxima in $\eta(t)$ in the left-hand panels, and times when $\eta(t) = 0$ down the right-hand side. We see that the vorticity field becomes increasingly braided as time increases, yet retains the same overall structure at corresponding points on the $\eta(t)$ curve. In a coarse-grained sense, at the minima/maxima the vorticity field has an M or W configuration in terms of the white regions, while at the zero-crossings the white and black regions are aligned in y. The physical picture shown earlier in Fig. 6 is too simplified to capture the case of fine structure in the critical layer; however we note that the dominant feedback on the normal mode component will occur precisely during the zero-crossings when this alignment takes place. Note that in the code (weak) viscosity is acting to smooth out fine-scale fluctuations in the vorticity field. The smoothing of such fine-scales is virtually irrelevant to the evolution of the amplitude $\eta(t)$ as it is forced by a term that integrates over the vorticity (recall (4.5)), and this is confirmed by the excellent agreement with the inviscid frequency in Fig. 11.

Finally we consider when a step is displaced by an amount $\beta\kappa$ from the centre $y = 0$ of the critical layer. This models the situation when the edge of a ring of vorticity is no longer exactly centred at $r = r_n$. If we set

$$\lambda_1^{\pm}(y) = \pm \mathrm{e}^{-(y/\kappa-\beta)^2} \quad \text{(up/down)}, \tag{5.12}$$

the solutions for $\eta(t)$ are complex-valued. The real part of the growth rate γ is shown in Fig. 13 as a function of κ, for a down-step with different values of β. It is seen that for each value of κ the quasi-mode remains stable as β is increased from zero and

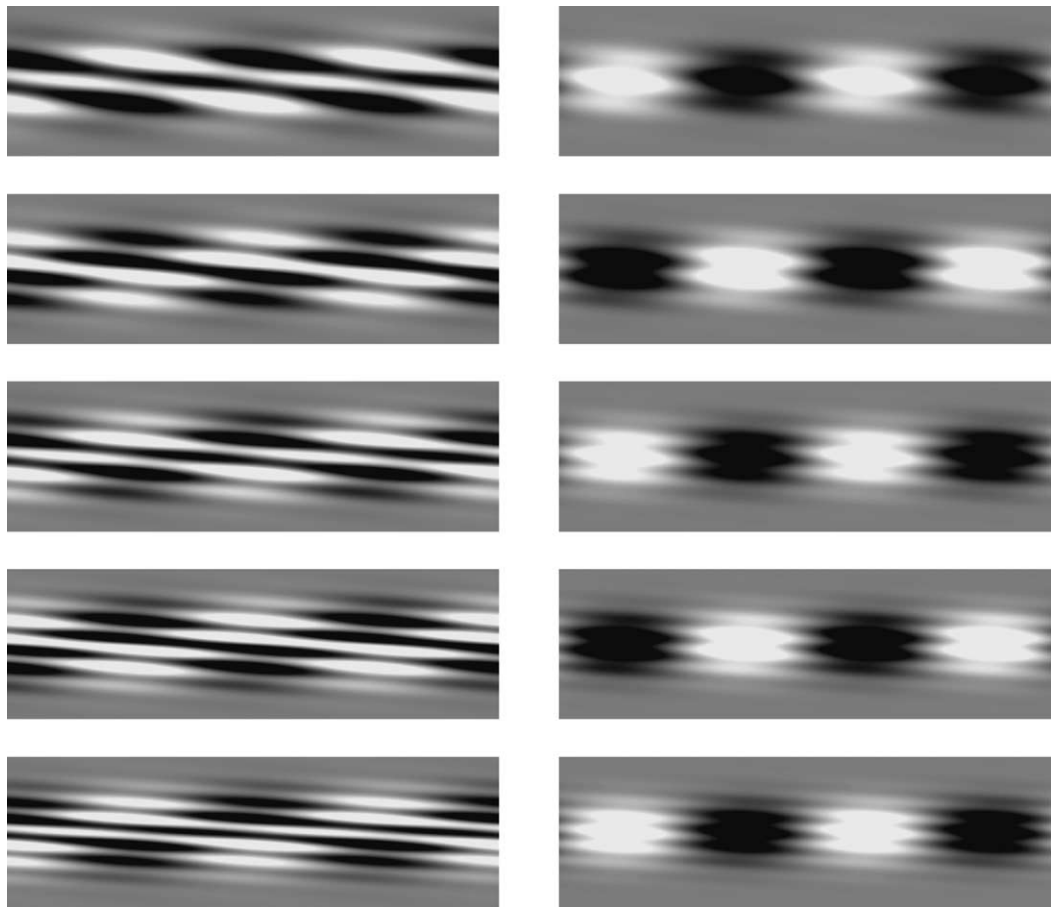

Fig. 12. Vorticity field $\omega(y,t)\,\mathrm{e}^{2\mathrm{i}\theta}$ + c.c. plotted in grey scale against (θ, y) for $0 < \theta < 2\pi$ and $-0.3 < y < 0.3$. The times are (a) $t = 20.4$, (b) $t = 23$, (c) $t = 25.6$, (d) $t = 28.1$, (e) $t = 30.7$, (f) $t = 33.2$, (g) $t = 35.8$, (h) $t = 38.3$, (i) $t = 40.9$ and (j) $t = 43.4$, corresponding as closely as possible to the maxima, minima and zeros of the amplitude of the quasi-mode. The sequence of plots starts in the top left and then proceeds left to right and top to bottom (times of maxima and minima appear in the left hand column, zeros in the right).

the step moves out of the critical layer, but the quasi-mode is less strongly damped. On the other hand, shifting an up-step away from the centre reduces the instability growth rate. Asymptotic results for large κ may be obtained from the dispersion relation

$$\gamma = \pm\pi\,\mathrm{erfc}(\gamma/n\kappa - \mathrm{i}\beta)\,\mathrm{e}^{(\gamma/n\kappa-\mathrm{i}\beta)^2} \quad \text{(up/down)} \tag{5.13}$$

giving

$$\mathrm{Re}\,\gamma = \pm\pi\,\mathrm{e}^{-\beta^2} - \pi^{3/2}\,\mathrm{e}^{-\beta^2}\left(1 - 4\beta\int_0^\beta \mathrm{e}^{u^2-\beta^2}\,\mathrm{d}u\right)\kappa^{-1} + \cdots \quad \text{(up/down)} \tag{5.14}$$

for $n = 2$, which is plotted in Fig. 13 with dots. The factor of $\exp(-\beta^2)$ that runs through the asymptotic result tells us that as we increase the displacement of the step from the centre of the critical layer the relevant growth or decay rate becomes exponentially small. It should be noted that we have considered only positive shifts β away from the centre of the critical layer: replacing β by $-\beta$ simply gives the complex conjugate growth rate γ, from the form of Eq. (5.13).

5.2. Bumps and troughs

We now consider the case of bumps and troughs of the fine-scale vorticity distribution in the critical layer. The forms $\lambda_2^{\pm}(y)$ we consider are given in (4.14) above (see also Fig. 7(e)–(h)). The dispersion relation becomes

$$\gamma = \mp\mathrm{i}\sqrt{2\pi\,\mathrm{e}}\left[1 - \sqrt{\pi}(\gamma/n\kappa)\,\mathrm{erfc}(\gamma/n\kappa)\,\mathrm{e}^{\gamma^2/n^2\kappa^2}\right] \quad \text{(bump/trough):} \tag{5.15}$$

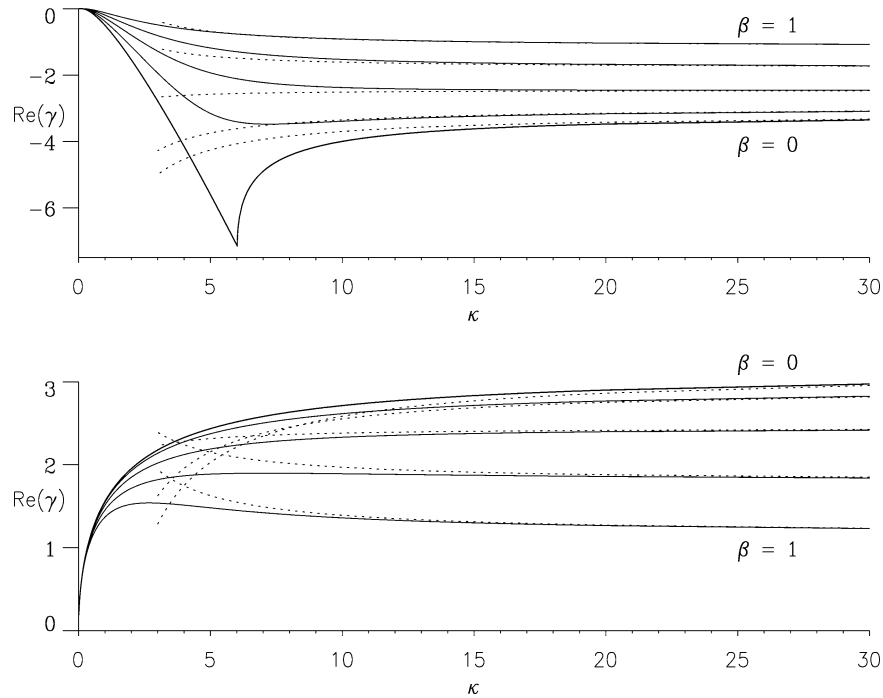

Fig. 13. Plot of $\mathrm{Re}\,\gamma$ against κ for different values of displacement β. Solid curves are numerical results for down-step $\lambda_1^-(y)$ (top plot) and up-step $\lambda_1^+(y)$ (lower plot), given by (5.12). Dashed curves show asymptotic behaviour given by (5.14). The displacement β takes the values $\beta = 0$, 0.25, 0.5, 0.75 and 1.0.

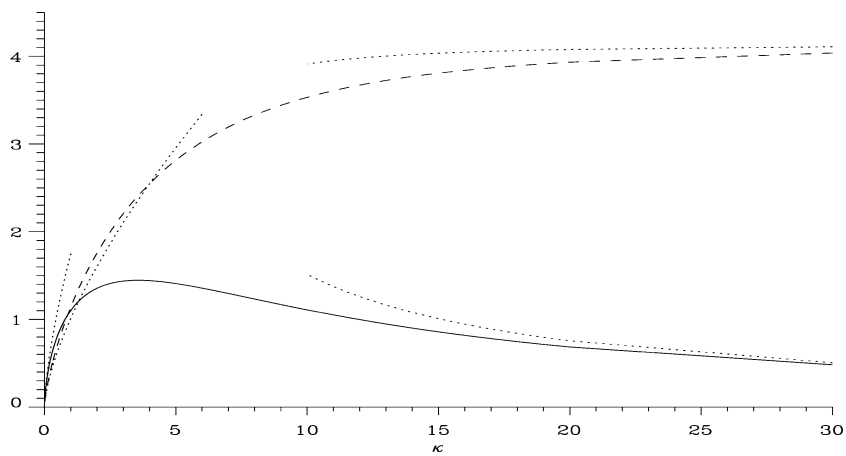

Fig. 14. Plot of $\mathrm{Re}\,\gamma$ (solid) and $\mathrm{Im}\,\gamma$ (dashed) as functions of κ for the trough profile (4.14b). The growth rates γ for a trough profile are the complex conjugate of those for the bump profile. Dotted lines show the asymptotic results (5.16) for small κ and (5.17) for large κ.

plainly the trough profile simply gives the complex conjugate growth rate of the equivalent bump profile, and so we focus on the case of a trough only. Results for growth rates are shown in Fig. 14 and are found by solving (5.15) numerically and asymptotically. The effect of the trough is to destabilise the quasi-mode, with $\mathrm{Re}\,\gamma > 0$ (solid curve) for the whole range of κ. Together with growth we have oscillations, since $\mathrm{Im}\,\gamma \neq 0$ (dashed curve).

We find asymptotic results (dotted curves on Fig. 14) by the same methods used to analyse the up-step and down-step. For $\kappa \ll 1$ and $n = 2$ we again use standard results from Chapter 7 of [38] to give

$$\gamma = \frac{1}{2}(\sqrt{3} \mp \mathrm{i})\sqrt{2}(\pi\,\mathrm{e})^{1/6}\kappa^{2/3} + \mathrm{O}\big(\kappa^{4/3}\big) \quad \text{(bump/trough)} \tag{5.16}$$

while if $\kappa \gg 1$

$$\gamma = \mp \mathrm{i}\sqrt{2\pi\,\mathrm{e}} + \mathrm{e}\pi^{3/2}\kappa^{-1} \mp \frac{1}{4}\mathrm{i}(2\pi\,\mathrm{e})^{3/2}(\pi+2)\kappa^{-2} + \mathrm{O}\big(\kappa^{-3}\big) \quad \text{(bump/trough)}. \tag{5.17}$$

These asymptotic results confirm that the amplitude of the quasi-mode possesses unstable oscillations for bumps or troughs in the critical layer.

6. Discussion

In this paper we have considered the stability and dynamics of vortices with sharp edges and additional fine structure at their periphery. Such vortices arise naturally through strongly nonlinear interactions in two-dimensional turbulence and in many geophysical applications. To understand issues of stability we have examined an idealised model of an isolated, axisymmetric vortex and excited non-axisymmetric motions by an impulsive strain. We obtain quasi-modes with damping or growth rates related to the magnitude of the vorticity gradient in the critical layer; note that for vortices in practical situations peripheral vorticity may seem weak in magnitude and so unimportant, but gradients can still be strong through stripping and merger processes. Obviously the significance of such instabilities depends on how the time-scale of growth or damping compares with other time-scales in a full dynamical problem, for example the time-scale between vortex collisions.

First we considered a family of isolated vortices varying from a smooth profile at one extreme to a top-hat vortex at the other. In the limit of the top-hat vortex, the dynamics is dominated by the vorticity distribution in a thin critical layer, where the angular velocity of the fluid flow is resonant with that of a normal mode. This mode can be considered as an elliptical distortion of the top-hat vortex and, depending on the vorticity gradient, positive or negative, the mode will be destabilised or stabilised, respectively. In the latter case the rebound phenomenon operates, and enstrophy is transferred from the non-axisymmetric components to the mean, as the elliptical distortion of the top-hat vortex decays with time by the mechanism depicted in Fig. 6. The evolution of the quasi-modes was explored numerically, and agreement with theory obtained [16,17,19].

We then discussed the role of fine structure within the critical layer by introducing steps, bumps and troughs in the basic axisymmetric vorticity profile. These model additional fine structure at the periphery of two-dimensional vortices. Using linear, inviscid theory, we have considered the effects of this additional structure on the structure and stability of the resulting quasi-modes. The results are summarised in Table 1 for the four different profiles and two particular limits. When κ (or, equivalently, w) is small, we obtain a narrow structure in the critical layer, while large values of κ give rise to a wide structure. In each case we have backed up our numerical studies with asymptotic analysis.

Let us focus first on the up-step and the down-step and, for definiteness and simplicity, take the compact vortex to be of top-hat type. These steps have the same effect as a uniform gradient in the critical layer in that they respectively destabilise and stabilise the normal mode, that is the elliptical distortion of the top-hat vortex. However, in the case of a down-step, as the scale κ of the step is reduced, we find that exponential decay is replaced by decaying oscillations. In the limit of a very small-scale step, the behaviour is primarily oscillatory with rather weak, exponentially small decay. These oscillations correspond to a complex conjugate pair of roots in the dispersion relation, and the normal-mode amplitude passes through zero periodically. In terms of a top-hat vortex, the vortex would oscillate through elliptical and circular states as it evolves, coupled to the critical layer. For a bump or a trough in the vorticity profile, centred on the critical layer, the effect is always destabilising, with oscillations. In this

Table 1
Table summarising the effect on quasi-modes of fine structure in the critical layer. A description of the profile in the critical layer is given, together with the analytical form $\Omega_{\mathrm{L}}(Y)$. The related parameters κ and w (with $\kappa = w/\mathcal{L}$) give the width of the fine structure

Description	$\Omega_{\mathrm{L}}(Y)$	w and κ	Growth or decay rate η	
			amplitude	frequency
Shallow up-step	$w\,\mathrm{erf}(Y/w)$	$\gg 1$	O(1) growth	
Sharp up-step	$w\,\mathrm{erf}(Y/w)$	$\ll 1$	$\mathrm{O}(\kappa^{1/2})$ growth	
Shallow down-step	$-w\,\mathrm{erf}(Y/w)$	$\gg 1$	O(1) decay	
Sharp down-step	$-w\,\mathrm{erf}(Y/w)$	$\ll 1$	Exp. weak decay	$\mathrm{O}(\kappa^{1/2})$
Broad bump	$w\,\mathrm{e}^{-Y^2/w^2}$	$\gg 1$	$\mathrm{O}(\kappa^{-1})$ growth	O(1)
Narrow bump	$w\,\mathrm{e}^{-Y^2/w^2}$	$\ll 1$	$\mathrm{O}(\kappa^{2/3})$ growth	$\mathrm{O}(\kappa^{2/3})$
Broad trough	$-w\,\mathrm{e}^{-Y^2/w^2}$	$\gg 1$	$\mathrm{O}(\kappa^{-1})$ growth	O(1)
Narrow trough	$-w\,\mathrm{e}^{-Y^2/w^2}$	$\ll 1$	$\mathrm{O}(\kappa^{2/3})$ growth	$\mathrm{O}(\kappa^{2/3})$

case there is a single complex root, not a conjugate pair, to the dispersion relation. This means a modified rotation rate of the normal mode; a top-hat vortex would carry a growing, rotating elliptical distortion, but not go through circular states.

There are several ways in which to extend the present study. One is to understand the results on fine structure in the critical layer in terms of Landau poles through analytic continuation of the normal mode equation in the complex plane [18,19]. Another possibility would be to consider the effects of viscosity. In this case we would introduce a driving force to maintain a given axisymmetric profile against viscosity, and then study the evolution of quasi-modes in a system such as (4.1) but with a viscous damping term on the right-hand side of the vorticity equation. This study is currently in progress. Moreover it would be of interest to investigate the effects of nonlinearity in the critical layer, building on the study of BLSY, in order to understand the dynamics of instabilities in vortices with fine structure at their edges. Simulations using, for example, contour dynamics techniques could complement predictions arising from nonlinear critical theory theory and thereby settle important issues such as whether the instability saturates. In the absence of the fine vorticity BLSY demonstrated that at sufficiently large amplitudes a cat's eye pattern forms and the vortex is permanently deformed to a tripolar structure.

Lastly, in practice vortices are often embedded within rotating strain fields. Here we have concentrated on the problem of an impulsive strain, but the study of other types, for example the ramped strain of [6] should be investigated, both in the theory developed and in fully nonlinear simulations.

Acknowledgements

We are happy to thank Dr. Konrad Bajer for a number of useful discussions, and Prof. David Dritschel who suggested we investigate the dynamics of vortices with sharp edges. The referees also made many helpful comments. I.H. is grateful to the UK EPSRC for support through a Research Studentship.

References

[1] M.E. Brachet, M. Meneguzzi, H. Politano, P.-L. Sulem, The dynamics of freely decaying two-dimensional turbulence, J. Fluid Mech. 194 (1988) 333–349.
[2] B. Fornberg, A numerical study of 2-d turbulence, J. Comput. Phys. 25 (1977) 1–31.
[3] J.C. McWilliams, The emergence of isolated coherent vortices in turbulent flow, J. Fluid Mech. 146 (1984) 21–43.
[4] L. Ting, R. Klein, Viscous Vortical Flows, Lecture Notes in Phys., Vol. 374, Springer, New York, 1991.
[5] B. Legras, D. Dritschel, Vortex stripping and the generation of high vorticity gradients in two-dimensional flows, Appl. Sci. Res. 51 (1993) 445–455.
[6] B. Legras, D.G. Dritschel, P. Caillol, The erosion of a distributed two-dimensional vortex in a background straining flow, J. Fluid Mech. 441 (2001) 369–398.
[7] J. Jiménez, A.A. Wray, P.G. Saffman, R.S. Rogallo, The structure of intense vorticity in isotropic turbulence, J. Fluid Mech. 255 (1993) 65–90.
[8] M.T. Montgomery, R.J. Kallenbach, A theory for vortex Rossby waves and its application to spiral bands and intensity changes in hurricanes, Q. J. R. Meteorol. Soc. 123 (1997) 435–465.
[9] T.A. Guinn, W.H. Schubert, Hurricane spiral bands, J. Atmos. Sci. 50 (1993) 3380–3403.
[10] G.B. Smith, M.T. Montgomery, Vortex axisymmetrization: dependence on azimuthal wave-number or asymmetric radial structure changes, Q. J. R. Meteorol. Soc. 121 (1995) 1615–1650.
[11] P. Haynes, Transport, stirring and mixing in the atmosphere, in: H. Chaté, E. Villermaux, J.-M. Chomaz (Eds.), Mixing, Chaos and Turbulence, Kluwer Academic, 1999.
[12] A.P. Bassom, A.D. Gilbert, The spiral wind-up of vorticity in an inviscid planar vortex, J. Fluid Mech. 371 (1998) 109–140.
[13] T.S. Lundgren, Strained spiral vortex model for turbulent fine structure, Phys. Fluids 25 (1982) 2193–2203.
[14] A.P. Bassom, A.D. Gilbert, The spiral wind-up and dissipation of vorticity and of a passive scalar in a strained planar vortex, J. Fluid Mech. 398 (1999) 245–270.
[15] C. Macaskill, A.P. Bassom, A.D. Gilbert, Nonlinear wind-up in a strained planar vortex, Eur. J. Mech. B Fluids 21 (2002) 293–306.
[16] N.J. Balmforth, S.G. Llewellyn Smith, W.R. Young, Disturbing vortices, J. Fluid Mech. 426 (2001) 95–133.
[17] S. Le Dizès, Non-axisymmetric vortices in two-dimensional flows, J. Fluid Mech. 406 (1999) 175–198.
[18] D.A. Schecter, D.H.E. Dubin, A.C. Cass, C.F. Driscoll, I.M. Lansky, T.M. O'Neil, The damping of asymmetries on a two-dimensional vortex, Phys. Fluids 12 (2000) 2397–2412.
[19] R.J. Briggs, J.D. Daugherty, R.H. Levy, Role of Landau damping in cross-field electron beams and inviscid shear flow, Phys. Fluids 13 (1970) 421–432.
[20] S. Kida, Motion of an elliptic vortex in a uniform shear flow, J. Phys. Soc. Japan 50 (1981) 3512–3520.
[21] A. Mariotti, B. Legras, D.G. Dritschel, Vortex stripping and the erosion of coherent structures in two-dimensional flows, Phys. Fluids 6 (1994) 3954–3962.
[22] C.F. Driscoll, K.S. Fine, Experiments on vortex dynamics in pure electron plasmas, Phys. Fluids B 2 (1990) 1359–1366.

[23] P. Koumoutsakos, Inviscid axisymmetrization of an elliptical vortex, J. Comput. Phys. 138 (1997) 821–857.
[24] M.V. Melander, J.C. McWilliams, N.J. Zabusky, Axisymmetrization and vorticity-gradient intensification of an isolated two-dimensional vortex through filamentation, J. Fluid Mech. 178 (1987) 137–159.
[25] D.G. Dritschel, D.W. Waugh, Quantification of the inelastic interaction of unequal vortices in 2-dimensional vortex dynamics, Phys. Fluids 4 (1992) 1737–1744.
[26] N.K.-R. Kevlahan, M. Farge, Vorticity filaments in two-dimensional turbulence: creation, stability and effect, J. Fluid Mech. 346 (1997) 49–76.
[27] A.H. Nielsen, X. He, J.J. Rasmussen, T. Bohr, Vortex merging and spectral cascade in two-dimensional flows, Phys. Fluids 3 (1996) 2263–2265.
[28] H.B. Yao, N.J. Zabusky, D.G. Dritschel, High-gradient phenomena in 2-dimensional vortex interactions, Phys. Fluids 7 (1995) 539–548.
[29] N.J. Balmforth, D. Del Castillo Negrete, W.R. Young, Dynamics of vorticity defects in shear, J. Fluid Mech. 333 (1996) 197–230.
[30] N.J. Balmforth, Stability of vorticity defects in viscous shear, J. Fluid Mech. 357 (1998) 199–224.
[31] D. Sipp, L. Jacquin, C. Cossu, Self-adaptation and viscous selection in concentrated two-dimensional vortex dipoles, Phys. Fluids 12 (2000) 245–248.
[32] K. Bajer, A.P. Bassom, A.D. Gilbert, Accelerated diffusion in the centre of a vortex, J. Fluid Mech. 437 (2001) 395–411.
[33] A.J. Bernoff, J.F. Lingevitch, Rapid relaxation of an axisymmetric vortex, Phys. Fluids 6 (1994) 3717–3723.
[34] H.K. Moffatt, H. Kamkar, The time-scale associated with flux explusion, in: A.M. Soward (Ed.), Stellar and Planetary Magnetism, Gordon & Breach, 1981, pp. 91–97.
[35] P.B. Rhines, W.R. Young, How rapidly is a passive scalar mixed within closed streamlines?, J. Fluid Mech. 133 (1983) 133–145.
[36] P.G. Drazin, W.H. Reid, Hydrodynamic Stability, Cambridge University Press, 1981.
[37] S.A. Maslowe, Critical layers in shear flows, Ann. Rev. Fluid Mech. 18 (1986) 405–432.
[38] M. Abramowitz, I.A. Stegun, Handbook of Mathematical Functions, Dover, 1965.